Coadsorption Model for First-Principle Description of Roles of Donors in Heterogeneous Ziegler-Natta Propylene Polymerization

Toshiaki Taniike* and Minoru Terano

School of Materials Science, Japan Advance Institute of Science and Technology, 1-1 Asahidai, Nomi, Ishikawa 923-1292, Japan

*CORRESPONDING AUTHOR

Tel: +81-761-51-1622; Fax: +81-761-51-1625; E-mail: taniike@jaist.ac.jp

ABSTRACT: Systematic periodic density functional calculations were conducted to clarify the mechanism for donors to exert steric and electronics influences on propylene polymerization using heterogeneous Ziegler-Natta catalysts. It was concluded that $TiCl_4$ preferentially adsorbs as mononuclear species on the $MgCl_2$ (110) surface and the coadsorption of donors with it is energetically viable. The coadsorption of donors on the (110) surface reinforces the electron density of the Ti mononuclear species, and sterically transfers the underlying C_2 symmetry to convert the originally aspecific mononuclear species into isospecific one. The nearest coadsorption of ethylbenzoate (EB) not only sterically induces the isospecificity of the Ti mononuclear species but also electrostatically improves the regiospecificity in propylene insertion. In addition, EB prevents sterically-demanding chain transfer to propylene, increasing the molecular weight of the produced polypropylene. Thus theoretically derived "coadsorption model" is highly consistent with a variety of experimentally known facts and believed to be useful for the *ab-initio* prediction of new donor structures.

KEYWORDS: Ziegler-Natta propylene polymerization; density functional theory; donor; mechanism; coadsorption; active site

1. Introduction

Since the discovery of Ziegler-Natta (ZN) olefin polymerization catalysts, tremendous researches and developments have continuously progressed their mechanistic understandings as well as commercial applications in the huge polyolefin field. Especially, developments of homogeneous metallocene and post-metallocene catalysts have opened new chemistry for precise olefin polymerization. For example, early or late transition metals combined with a variety of tailored ligands have enabled stereo- and regio-selective living polymerization of various olefins, incorporation of branches as well as bulky and polar groups into polyolefin backbone, stereo/chemo block/gradient copolymerization, and so on [1-11]. Aside from these extensive progresses in homogeneous catalysis, traditional heterogeneous ZN catalysts still keep the top priority in the industrial olefin polymerization, especially accounting for more than 99% of about 50 million tons/year of isotactic polypropylene (iPP) over the world.

The key technology of heterogeneous ZN catalysts for the iPP production is at the concomitant usage of $MgCl_2$ support and organic electron donors [12]. $MgCl_2$ enhances both the concentration of active Ti species and their activity [13,14], while donors bring about dramatic improvement of the stereospecificity of the catalysts as well as significant alternation of other catalytic properties such as the productivity, hydrogen response, comonomer incorporation efficiency, and molecular weight distribution (MWD) of produced iPP [15,16]. Continuous developments over three decades have invented four families of donor systems, that is, the first benzoate/benzoate, most widely used phthalate/alkoxysilane, 1,3-diether/(alkoxysilane) featured with high hydrogen response, and succinate/alkoxysilane for broader MWD. Thus, one can say that catalytic performances of heterogeneous ZN catalysts can be altered based on the

combination of different internal and external donors with $MgCl_2$, in contrast to the metal-ligands combination for homogeneous catalysts. However, the largest difference between the heterogeneous and homogeneous catalysts is attributed to the absence of a clear answer for how the combination of specific donors with $MgCl_2$ controls the catalytic properties of active Ti species.

Activated $MgCl_2$ as catalyst support usually has δ-form, characterized with small dimensions of Cl-Mg-Cl tri-layers disorderly stacked along the [001] direction [17,18]. Its most stable (001) basal plane is coordinatively saturated [19] and inactive to the adsorption of $TiCl_4$ [20,21] (*i.e.* catalytically irrelevant). Catalytically relevant surfaces are low-index planes that expose unsaturated Mg^{2+} ions. Especially, the (110) and (100) lateral planes have been long believed as representative ones [17,18] (we employ the crystallographic notation of (100) rather than (104) [19] in order to stand on the same ground with historical discussion). While the dominant exposure of the (100) lateral planes is estimated for equilibrium crystallographic morphology of $MgCl_2$ [19], activated $MgCl_2$ can also have the (110) lateral plane, presumably as a result of non-equilibration or equilibration shifted in the presence of adsorbates such as $TiCl_4$ and donors. Mori et al. observed with transmission electron microscope that lateral surfaces of mechanically activated $MgCl_2$ are dominantly composed by the (110) and (100) planes [22], while Andoni et al. reported preferential growth of $MgCl_2$ crystal along the [110] direction in the presence of 1,3-diether [23]. Recent density functional theory (DFT) calculations exactly pointed out shifted equilibrium, where the (110) termination prevailed the (100) termination in the presence of ether adsorbates [24].

Structures of surface $TiCl_4$ species and active sites have been discussed based on the $MgCl_2$

(110) and (100) surfaces. $TiCl_4$ epitaxially adsorbs on these $MgCl_2$ surfaces due to similar ionic radii between Ti^{4+} and Mg^{2+}, bearing $TiCl_4$ mononuclear species on the (110) surface and Ti_2Cl_8 dinuclear species on the (100) surface [25]. Active sites for propylene polymerization are regarded as monoalkylated trivalent Ti species [15,26-28], resulting from extraction and alkyl substitution of terminal Cl atoms with alkylaluminum activator. In analogous to the first and second generation $TiCl_3$ catalysts [29,30], the mononuclear species on the (110) surface and the dinuclear species on the (100) surface were respectively assigned as aspecific and isospecific active sites [25]. Although the nuclearity of surface $TiCl_4$ species has not been experimentally concluded yet [31-33], most of DFT studies have agreed on the energetic preference of the $TiCl_4$ mononuclear species on the (110) surface [34-39].

On the mechanism of stereospecific improvements by the addition of donors, the first microscopic proposal was made by Busico, Corradini and their coworkers [25]. They proposed that four-fold coordinated Mg^{2+} ions on the (110) surface are preferentially poisoned by selective adsorption of donors, which prevents the formation of the aspecific mononuclear species on the (110) surface and increases the fraction of the isospecific dinuclear species on the (100) surface. The proposal implicitly assumes that isospecific active sites are the same dinuclear species irrespectively of donor structures, and the degree of the stereospecific improvement depends on the selectivity of the donor adsorption on the (110) surface. Afterwards, it became clear that polymer microstructures reflecting active site structures are sensitive to donor structures [40-45], suggesting that donor molecules are directly involved in the active sites. Since the coordination of donor molecules to $TiCl_4$ is spectroscopically excluded [46], researchers now agree that donor molecules adsorb on $MgCl_2$ surfaces and

interact with nearby Ti species in a non-bonded manner to improve the stereospecificity of the Ti species. Busico et al. postulated a three-site model as a versatile active site image in $MgCl_2$-supported ZN catalysts [47], which was later modified by Terano et al. [48]. The three-site model describes the stereospecificity of supported Ti species irrespectively of their location ((110) or (100)) and nuclearity (mononuclear or dinuclear) but according to the absence or presence of bulky ligands, $L_{1,2}$, (Cl or donor) at the neighboring undercoordinated metal sites (Mg, Ti or Al). Since the Ti dinuclear species on the (100) surface does not have any coordinative unsaturation at the neighboring metal sites, alternative idea becomes increasingly predominant that donors coadsorb with the Ti mononuclear species on the (110) surface to convert it into an isospecific active site [49-52]. Recent cluster DFT calculations firstly proved that the coadsorption of two succinate molecules at the L_1 and L_2 positions can convert the aspecific Ti mononuclear species into isospecific one on the $MgCl_2$ (110) surface [49].

Based on these backgrounds, it is plausible that the coadsorption of donors modifies the catalytic performances of the Ti mononuclear species on the $MgCl_2$ (110) surface. However, the idea is still evidenced by few aspects such as stronger adsorption of $TiCl_4$ on the (110) surface [34-38] and the presence of coordination vacancies at $L_{1,2}$ on the same surface. Many other aspects remain unclarified such as energetic feasibility of the coadsorption of donors, electronic and steric interactions upon the coadsorption, and their influences not only on the stereospecificity but also on other catalytic properties like regiospecificity and molecular weight.

The aim of the present study is to offer a convincing conclusion on the mechanism for donors to modify the polymerization performance of ZN catalysts by means of systematic periodic DFT

calculations. For this purpose, we have performed a reliable level and amount of DFT calculations and to compare the obtained results with a number of previous experimental results. In the former part, results are presented and discussed for the independent adsorption of $TiCl_4$ and donors as well as their coadsorption and resultant interactions on the $MgCl_2$ (110) and (100) surfaces. The obtained conclusions support the coadsorption of donors with Ti mononuclear species on the (110) surface from viewpoints of the energetic stability and consistency with experimental facts. In the latter part, the influences of the coadsorption of ethylbenzoate (EB) as the simplest industrial donor were systematically examined on the polymerization performance of the Ti mononuclear species. We found that the coadsorption of EB not only converts the aspecific Ti mononuclear species into isospecific one, but also accounts for experimentally known enhancements in the regiospecificity and polymer molecular weight [44,45,55,56]. Thus, the present article proposes that the coadsorption of donors on the (110) surface is theoretically and experimentally highly consistent, and enables the first comprehensive molecular-level description of the role of donors.

2. Numerical

All the DFT calculations were performed in a spin unrestricted manner using the DMol3 package [57]. The Perdew-Burke-Ernzerhof (PBE) functional [58] was chosen, since PBE gave the best agreement with the experimental activation energies of olefin insertion among several functionals of the generalized gradient approximation (GGA) type. However, it is notable that other functionals such as PW91 [59], BP [59,60], and BLYP [60,61] provided similar conclusions to PBE in a qualitative meaning. A double numerical polarized (DNP) basis set [57]

was employed together with effective core potentials [62,63]. DMol3 instructs that the numerical basis sets are designed to minimize the basis set superposition error. The convergence criteria for normal geometry optimization were set to 0.01255 kcal/mol in energy and 2.510 kcal/mol·Å in force.

As in our previous studies [34,51,52], the most stable α-crystalline phase was assumed for the $MgCl_2$ bulk, and its (110) and (100) lateral surfaces were employed as catalytically representative cuts. Recently, Busico et al. reported the instability of the bulk-terminated (100) surface compared to the (104) surface, based on dispersion-corrected DFT calculations [19]. On the other hand, Boero et al. showed that the bulk-terminated (100) surface reconstructs in a way that terminal Cl atoms migrate to coordinate tri-coordinated Mg atoms [38]. The resultant (100) surface exposed only penta-coordinated Mg atoms on the surface, similarly to the (104) surface [38]. The (100) surface employed in this study corresponds to the reconstructed one with similar stability to the (104) surface. The (110) and (100) surfaces were expressed by the slab model with 1.5 nm of a vacuum layer. A p(2x2) unit cell of 6 atomic layer thickness (composed of 24 $MgCl_2$ units) was used for the (110) surface, and a p(3x1) unit cell of 14 atomic layer thickness (composed of 36 $MgCl_2$ units) for the (100) surface. A p(4x1) unit cell with the same thickness was employed only for $TiCl_4$ dinuclear species on the (100) surface. 2 x 1 x 1 *k*-point mesh was applied to the p(3x1) (100) unit cell, while the gamma point was used for the other unit cells. Both the thickness of the unit cells and the density of the *k*-points were determined in terms of the converged adsorption energies of $TiCl_4$ and $TiCl_3$ mononuclear species on the $MgCl_2$ surfaces [34,51]. Also, the widths of the unit cells were decided not to have direct steric interactions between adsorbates in neighboring cells. It is notable that small clusters composed

of several to 10 $MgCl_2$ units could not correctly describe electronic interaction with Ti species, suggesting the necessity of a large unit cell for reliably expressing the nature of the $MgCl_2$ surfaces. The $MgCl_2$ slabs were fully relaxed except the bottom two atomic layers fixed in their bulk positions during geometry optimization and transition state search.

It has been widely accepted that active sites of ZN catalysts for propylene polymerization are monoalkylated trivalent Ti species [15,26-28]. Though tetravalent species also has a high activity for propylene polymerization as in group IV metallocene catalysts, $TiCl_4$ which is usually situated in an octahedral symmetry on $MgCl_2$ [31-33,64] might be difficult to offer a vacant site for monomer coordination. Here isobutyl (*i*Bu) or methyl (Me) was employed as the alkyl group, *i.e.* as the growing chain. *i*Bu is the minimal unit to describe the growing chain in a sequence of the 1,2 insertion of propylene. Based on ^{13}C-NMR chain end analyses using ^{13}C-enriced alkylaluminum, it was clarified that the stereoselectivity of the propylene insertion into *i*Bu-Ti was as high as those observed in the growing chain [40,41]. On the contrary, the first propylene insertion into shorter alkyl-Ti was less stereoselective [40,41]. In this way, the size of the alkyl group is important to convey the site chirality to inserting propylene, and the smallest Me (*i.e.* the least effects from the site chirality) was useful for us to investigate electronic influences of donors.

Generally, alkyl-Ti and olefin can undergo two kinds of reactions in polymerization: insertion for the chain growth, which follows the Cossee-Arlman mechanism [65] assisted with agostic interaction [66], and chain transfer for the termination of the chain growth, where monomer extracts β-hydrogen of a growing chain to renew the growing chain. Both of the reactions go through π complexation between the Ti center and olefin. In this study, transition states of the

insertion and chain transfer to propylene were evaluated for all possible pathways which differ from each other in terms of the configurations of the growing chain and monomer. For example, four insertion pathways, namely, 1,2-*re*, 1,2-*si*, 2,1-*re*, and 2,1-*si*, exist for the propylene insertion into Me-Ti. The same number of pathways exists for the propylene insertion into *i*Bu-Ti for each configuration of *i*Bu. Transition states for the propylene insertion were approximated at the energy maxima along a reaction coordinate, the C_2-C_α distance for the 1,2 insertion and the C_1-C_α distance for the 2,1 insertion. The reaction coordinate was scanned over 2.0-2.6 Å with a step size of 0.05 or 0.1 Å. As the potential energy profiles of olefin insertion are flat along the reaction coordinate [49,67], such the linear scan was believed to be accurate enough for the identification of the transition states. The energy maxima were mostly obtained in the range of 2.1-2.3 Å of the reaction coordinate [49,67-69]. As for the transition states of the chain transfer to propylene, the reaction coordinates were assumed as the C_2-H_β distance for the 1,2 orientation and the C_1-H_β distance for the 2,1 orientation. First, approximate transition states were similarly decided at the energy maxima along the reaction coordinates, where the potential energy profiles were relatively steep. Then, accurate transition states were searched in a way to satisfy the energy maximum for the normal mode corresponding to the reaction coordinates and the energy minima for the other normal modes, starting from numerically derived Hessian matrices of the approximate transition states. The higher convergence criteria (0.01255 kcal/mol in energy and 0.6275 kcal/mol·Å) were employed in the geometry optimization and transition state search relating to the resting states, π complexation, insertion and chain transfer, in order to improve the accuracy of energetic values.

In this study, activation energies of the insertion and chain transfer were given as apparent

values, which are defined as the energetic difference between resting states as the starting point of a catalytic cycle and transition states. Apparent activation energies are normally equal to those experimentally obtained from the Arrhenius plots for heterogeneous catalysis, as long as the adsorption of reagents onto active sites is far from being saturated, which is the case for ZN olefin polymerization under usual conditions [14,70]. We have neglected the contributions of entropy and zero-point vibration in the reactions, in cost of the relatively large unit cells. However, in separate calculations using $MgCl_2$ clusters with tractable sizes, these contributions were mostly constant among different pathways for the insertion and chain transfer: about 16-17 kcal/mol at 350 K for the entropy and about –1 kcal/mol for the zero-point vibration. Similar insensitivities were previously reported by Ziegler and his coworkers [70,71]. Consequently, the energies of arbitrary two pathways were believed to be nicely compared even without those contributions, for example, in estimating the stereo- and regio-selectivities of propylene insertion, the most probable molecular weight, and so on.

In the end of this section, we would like to mention the computational accuracy. Judging from experimentally known selectivities for the propylene insertion with ZN catalysts, energies around a few kcal/mol become important. Although a few kcal/mol in an absolute energy is beyond the accuracy of the employed method, it is expected that differential energies which determine selectivities are more accurate due to error cancellation between two absolute energies. With a similar reason, it is believed that influences of donors on the propylene polymerization properties are safely discussed in terms of relative energies. Moreover, by calculating activation energies among many different pathways, safe tendency must be derived for the influences of donors on the polymerization properties. Such a comprehensive DFT

survey with a sufficiently large $MgCl_2$ model has been scarcely implemented for ZN catalysts, and this is one of the purposes of the present DFT calculations.

3. Results and discussion

3.1. States of $TiCl_4$ and donors on $MgCl_2$

3.1.1. Energetic aspect

When one infers the mechanism for donors to improve the catalyst stereospecificity, the states of $TiCl_4$ and donors on catalyst surfaces must be considered. $TiCl_4$ can adsorb on the $MgCl_2$ (110) surface only as the mononuclear species (Fig. 1a). The adsorption energy calculated by us was –20 kcal/mol (Table 1). On the other hand, $TiCl_4$ accepts both the mononuclear and dinuclear forms on the (100) surface (Figs. 1b and 1c). Their adsorption energies (per Ti) were respectively –13 and –11 kcal/mol, both of which were much smaller than that on the (110) surface (Table 1). Many of previous calculations reported similar trends for the adsorption energies of $TiCl_4$ on the $MgCl_2$ (110) and (100) surfaces [34-38], even though energetic magnitudes were more or less dependent on exchange-correlation functionals. Thus, it seems clear that $TiCl_4$ adsorbs more strongly on the (110) surface. It is noticeable that the most recent calculations by D'Amore et al. based on the-state-of-the-art exchange correlation functionals concluded only the (110) surface can bind $TiCl_4$ [39].

Ester-type donors show similar adsorption energies on the (110) and (100) surfaces (Fig. 2 and Table 1). Monofunctional benzoate adsorbs with a monodentate structure on both of the surfaces, giving *ca.* –30 kcal/mol of the adsorption energies. Bifunctional phthalate and succinate can adsorb either as a bidentate structure or as bridging structures on the (110) surface,

while only a (intra-layer) bridging structure is allowed on the (100) surface. The adsorption energies of these diesters are about –30-40 kcal/mol, irrespectively of the adsorption mode and the surface type. On the contrary, 1,3-diether adsorbs only with a bidentate structure on the (110) surface due to its short oxygen-oxygen distance, giving –31 kcal/mol of the adsorption energies, while the adsorption energy on the (100) surface was less than half. The results in Table 1 are completely in line with recent DFT calculations by Correa et al. [49].

The surface-selective adsorption of 1,3-diethers was previously employed to support the hypothesis of the formation of the isospecific dinuclear species on (100) through the selective poisoning of (110) [72]. However, recent experimental results [23] reported preferential growth of one kind of lateral surfaces in the presence of 1,3-diether. The obtained lateral surfaces were assigned by them as the (110) surface, since 1,3-diether selectively adsorbs and stabilizes the (110) surface so as to induce its selective exposure. Thus, it appears problematic to assume the co-exposure of the (110) and (100) surfaces in certain cases. Instead, it is necessary to consider the role of internal donors in catalyst preparation to understand the states of $TiCl_4$ and donors on $MgCl_2$ support. In general, preparation of ZN catalysts accompanies the fabrication of activated $MgCl_2$ support in the presence of $TiCl_4$ and/or internal donor at an elevated temperature. Activated $MgCl_2$ support is featured not only with great structural disorder along the [001] direction [17] but also with small crystalline dimensions [18], which plausibly result from the stabilization of lateral surfaces by the adsorption of $TiCl_4$ and internal donor. Consequently, it is expected that the adsorption behaviors of $TiCl_4$ and internal donors strongly affect the structure of $MgCl_2$ support. For example, in the presence of an adsorbate which prefers the (110) surface (such as 1,3-diether), the (110) surface is supposed to be preferentially stabilized and exposed.

On the contrary, in the presence of a non-selective adsorbate (ester-type donors), both the (110) and (100) surfaces are supposed to be similarly stabilized and exposed. The experimental report by Andoni et al. [23] supports the above discussion: in the presence of non-selective ester-type donors, the morphology of $MgCl_2$ became rectangular, indicating the co-presence of the (110) and (100) lateral cuts, while only hexagonal morphologies were obtained in the presence of selective 1,3-diether, corresponding to the preferential exposure of (110). When both the (110) and (100) surfaces are exposed for ester-type donors, $TiCl_4$ is supposed to preferentially replace an internal donor on the (110) surface, due to the preferential adsorption of $TiCl_4$ on (110). On the other hand, $TiCl_4$ necessarily attaches to the (110) surface when 1,3-diether is employed as an internal donor.

Provided that an internal donor induces the exposure of both/either the (110) and/or (100) surfaces, it is important to consider the states and interactions of $TiCl_4$ and donors on these two surfaces. Recently, we have reported that there is no significant attraction or repulsion between $TiCl_4$ and EB on the two $MgCl_2$ surfaces [51,52], and that they tend to coadsorb close to one another at a high surface coverage, which is the case for real catalysts containing as many as one $TiCl_4$ and donor molecules per 10-20 $MgCl_2$ units [15]. Considering the result that $TiCl_4$ adsorbs more strongly on the (110) surface as the mononuclear species, coadsorption of mononuclear $TiCl_4$ with donors on the $MgCl_2$ (110) surface is concluded as energetically the most plausible scenario.

3.1.2. Electronic aspect

Electronic interactions among $MgCl_2$, $TiCl_4$ and donors are totally different between the (110)

and (100) surfaces. In our previous DFT calculations [51,52], it was found that the $MgCl_2$ (110) surface donates much more electron density into $TiCl_4$ than the (100) surface. Moreover, coadsorption of EB further reinforced the electron density of $TiCl_4$ on the (110) surface, while electron supplied from donors to $MgCl_2$ support was hardly transferred into $TiCl_4$ on the (100) surface. Soga and Shiono examined the electron density of Ti species supported on various halides with X-ray photoelectron spectroscopy (XPS) and concluded that one of the advantages of $MgCl_2$ as a support is attributed to its high electron donation ability [53]. In addition, Zhao et al. clarified with XPS that internal donors further enhance the electron density of Ti centers [54]. In these points of view, $TiCl_4$ coadsorbed with donors on the (110) surface fulfills the experimentally obtained electronic aspects, and consequently regarded to be catalytically more important species than that on the (100) surface.

3.1.3. Steric aspect

Isoselective propylene polymerization is generally catalyzed by a C_2 (or C_1) symmetric active site. In typical metallocene catalysts, a C_2 symmetric space is generated around a metal center by the coordination of bridged cyclopentadienyl ligands. In ZN catalysts, the epitaxial adsorption of $TiCl_4$ induces a C_2 symmetry around Ti due to the structure of $MgCl_2$ surfaces, which is the case for the mononuclear species on the (110) surface and the dinuclear species on the (100) surface. In spite of the adequate symmetry, the Ti mononuclear species is aspecific owing to the lack of the stereo-regulating ligands at $L_{1,2}$ [47]. On the contrary, the dinuclear species is classified as an isospecific site due to the presence of Cl ligands at $L_{1,2}$ [47]. As was mentioned in the introduction, polymer microstructure analyses led to a conclusion that donors

interact with nearby Ti species and form new isospecific active sites, whose performances are sensitive to the molecular structures of donors [40-45]. On the other hand, it is known that agglomeration of Ti species progresses in the course of the reduction of $TiCl_4$ into Ti^{3+} and Ti^{2+} by reacting with alkylaluminum. An electron spin resonance (ESR) study by Sergeev et al. revealed that the population of ESR-active Ti^{3+} mononuclear species was greatly enhanced by the addition of donors [73]. We have recently found that isolated Ti mononuclear species is much less isospecific than agglomerated Ti species in the absence of donors, but the isolated Ti species is more efficiently converted into highly isospecific sites upon the addition of donors [43]. These suggest that donors not only prevent the agglomeration of Ti species but also increase the isospecificity of the Ti mononuclear species. At this point, we have reached a hypothesis that the coadsorption of donors generally occurs with the $TiCl_4$ mononuclear species on the (110) surface.

Based on these backgrounds, we describe here how donors improve the isospecificity of the Ti mononuclear species through their random adsorption [51,52] on the (110) surface, using an illustration with quadrants introduced by Correa et al. [49]. Originally, the C_2 symmetry of the Ti mononuclear species on the (110) surface arises from the fact that the O_h axes of the Ti center projected on the surface obliquely cross with $MgCl_2$ tri-layers, as shown in Fig. 3a. Consequently, the reaction spaces around the Ti center illustrated by white and gray quadrants in Fig. 3a (right) are necessarily non-equivalent, which gives a two-fold rotation axis at the Ti center without mirror planes (*i.e.* C_2 symmetric). However, the Ti mononuclear species is still aspecific due to the absence of steric hindrance that transfers the underlying symmetry to the growing chain and monomer. In other words, the growing chain and monomer cannot

distinguish the two kinds of the quadrants without appropriate steric hindrance.

When one considers coadsorption of donors with the Ti mononuclear species, ester-type donors can be energetically non-selectively placed at sites S_A-$S_{E'}$ in Fig. 3a [51,52]. However, steric impacts of coadsorbed donors depend on the coadsorption sites. Donors placed at the sites S_A and $S_{A'}$ are sterically the most important due to the shortest carbonyl-Ti distance, while steric influences from the other sites are regarded as secondary otherwise negligible. This situation is illustrated in Fig. 3b. Among ester molecules non-selectively distributed at S_A-$S_{E'}$, molecules placed at S_A and $S_{A'}$ occupy the gray quadrants and force the growing chain and monomer to orient into the white quadrants. On the other hand, diether-type donors can coadsorb at the sites S_B-$S_{E'}$ except S_A and $S_{A'}$ through the bidentate coordination again in a non-selective manner. The sterically most important locations are S_C and $S_{C'}$, while the coadsorption at S_E and $S_{E'}$ may have some level of influences. Thus, diester molecules occupy the white quadrants to orient the growing chain and monomer into the gray quadrants (Fig. 3c). On the contrary, the axes of the Ti mononuclear species projected on the (100) surface are parallel or perpendicular to the $MgCl_2$ layers, and therefore coadsorption of donors cannot induce a C_2 symmetry on the (100) surface.

In this way, the coadsorption of donors with the Ti mononuclear species on the (110) surface is not only energetically and electronically advantageous, but also compatible with the enhancement of the isospecificity. Coadsorbed donors sterically transfer the C_2 symmetry of the Ti mononuclear species on the (110) surface to the growing chain and monomer so as to convert an originally aspecific site into an isospecific one, which is automatically achieved as a result of non-site-selective coadsorption of donors.

3.2. Influences of donors on the resting state

We have postulated the importance of the coadsorption of donors with the Ti mononuclear species on the (110) surface in **3.1**. Of course, it must not be the sole surface state of ZN catalysts, exhibiting a variety of surface heterogeneity [43]. For example, the dominance of agglomerated Ti species in the absence of donors suggests the location of Ti species on the (100) surface, whose fraction is largely reduced but still remains in the presence of donors [73]. Thus, we do not exclude the presence of the other Ti species (e.g. the dinuclear species on the (100) surface), but regard the coadsorption on the (110) surface as the most plausible state in the presence of donors. Hereafter, taking EB as the simplest example of industrial donors, we describe the electric and steric influences of coadsorption on the activity, stereospecificity, and regiospecificity of propylene polymerization. For this purpose, one EB molecule was placed at the sterically most important site, S_A (Fig. 3a), and incoming propylene was placed in the opposite side of EB, based on the fact that steric influences of EB are mainly imposed on the much bulkier growing chain [74]. The second EB molecule would be required at the site $S_{A'}$ for the second insertion, which was not considered in this study.

First, influences of EB were examined for the resting state (corresponding to the starting point of the catalytic polymerization cycle). Fig. 4 illustrates four possible conformations of the resting state in the presence of EB. Similar four conformations also exist in the absence of EB (not shown). All the conformations possess agostic interactions, characterized by elongated C-H distances compared with a typical C-H distance of 1.10 Å. The conformations in Figs. 4a and 4b possess weak α-agostic interactions with the corresponding C-H distances elongated into

1.11-1.12 Å. They differ in the orientation of C_β of the growing chain (right and left), and are precursors for the α-agostic assisted insertion. The conformations in Figs. 4c and 4d possess strong β-agostic interaction with the corresponding C-H distances elongated into 1.14-1.15 Å. They differ in the orientation of C_β (back and front), and are precursors for the β-agostic assisted insertion and the chain transfer to monomer. Conformations with γ-agostic interactions as a direct product of the α-agostic assisted insertion [75,76] were not considered due to the limitation of the *i*Bu growing chain. For all the conformations, the symmetry is trigonal bipyramidal (TBP) rather than O_h.

Table 2 summarizes the relative stability of each conformation with respect to the most stable β-agostic conformation in the absence of EB, where each conformation is denoted according to the type of the agostic interaction and to the orientation of C_β. The relative stabilities of the conformations in the presence of EB were derived by $\{E(TiCl_2iBu/EB/MgCl_2) - E(TiCl_2iBu/MgCl_2)\} - \{E(TiCl_3/EB/MgCl_2) - E(TiCl_3/MgCl_2)\}$. Since the stability of $TiCl_3$ is similar with and without EB (corresponding to a marginal coadsorption energy [51,52]), the obtained values mostly comprise of the energetic difference of $TiCl_2$*i*Bu with and without EB. In the absence of EB, the most stable conformations are those with the β-agostic interaction, while the α-agostic conformations are about 4 kcal/mol less stable. The orientation of C_β did not affect the stability for both the β- and α-agostic conformations. The nearest coadsorption of EB destabilized the β- and α-agostic conformations by *ca.* 5 kcal/mol and by *ca.* 3 kcal/mol, respectively. Since the degrees of the destabilizations were rather insensitive to the orientation of C_β for both the β- and α-agostic conformations, the influence of EB on the resting state was concluded as mostly electrostatic. This was also supported by the fact that the least bulky Me

was destabilized by EB similarly to the α-agostic conformations. The coadsorption of EB enriches the electron density of Ti species on the (110) surface. As a result, alkyl groups with poor electron affinity are destabilized and the agostic interactions are weakened. The destabilization was more obvious for the β-agostic conformations with stronger agostic interactions.

The values in the parentheses in Table 2 show the equilibrium population of each conformation, calculated based on the Arrhenius law at 350 K (a typical polymerization temperature). Since the transformation of the β-agostic conformations into the α-agostic conformations required only 5-6 kcal/mol of the activation energies (much lower than the free energy of the insertion), mutual transformation among different conformations was regarded to be fast enough to achieve the equilibrium population. Both in the absence and presence of EB, the β-agostic conformations dominate. However, EB increased the populations of the α-agostic conformations by a factor of 10, suggesting that EB may restrict the β-agostic assisted insertion and the chain transfer to monomer compared with the α-agostic assisted insertion.

3.3. Influences of donors on the π complex

Second, influences of EB on the π complexation of propylene were examined. Fig. 5 shows the structures of the π complexes which were examined in this study. Propylene preferentially coordinates to Ti^{3+} with its double bond aligned perpendicularly to the Ti-C_α bond [77]. π complexes with the double bond aligned parallel to the Ti-C_α bond also formed saddle points, but they were always 1-3 kcal/mol less stable than those with the perpendicular alignment and not shown here. For each conformation of the resting state, four orientations of propylene were

calculated, where the methyl group of propylene was placed at either of $R_{1\text{-}4}$. The position of the methyl group at C_β was also varied (at either R_A or R_B) for the α-agostic conformations. In the presence of EB, propylene was attached to the opposite side of EB, while the growing chain was inclined to the side of EB.

For the simplest instruction, the adsorption of ethylene, propylene and fluoroethylene (C_2H_3F) to $TiCl_2Me$ was first studied in the absence of EB, and their adsorption energies (ΔE_{ad}) are summarized in Table 3. ΔE_{ad} for ethylene was calculated to be –9.45 kcal/mol, in rough agreement with the previous DFT calculation (–7.3 kcal/mol) by Cavallo et al. [68] in spite of differences in the functional and the model size. The ΔE_{ad} values of propylene and fluoroethylene were insensitive to the positions ($R_{1\text{-}4}$) of the methyl and fluorine substituents, and on average –8.62 and –6.37 kcal/mol, respectively. Thus, the presence of the substituents weakened the binding of olefins, which was more obvious for electron withdrawing fluorine than for the electron donating methyl group. This fact suggests that the π electron donation to Ti^{3+} is important for the adsorption of olefins to Ti^{3+}. The slightly weaker binding of propylene than ethylene is likely attributed to the steric reason. The ΔE_{ad} values for the same three kinds of olefins in the presence of EB are shown in Table 4. The coadsorption of EB weakened the binding of ethylene, propylene and fluoroethylene by 1.5, 2.4, and 1.0 kcal/mol on average, respectively, which resulted from the competitive electron donations from EB and olefin into $TiCl_2Me$.

The replacement of Ti-Me with Ti-*i*Bu largely weakened the binding of propylene. In the absence of EB, the average ΔE_{ad} value was –2.83 kcal/mol for Ti-*i*Bu as compared with –8.62 kcal/mol for Ti-Me (Table 3). Both the stabilization of the resting state through the β-agostic

interaction and the increased bulkiness around Ti mostly account for this reduction. The most stable species were π complexes with the β-agostic conformation (back), giving the average ΔE_{ad} value of –5.40 kcal/mol. The π complexation with the β-agostic conformation (front) was less stable due to steric interference between H_β and propylene. The magnitudes of ΔE_{ad} for the α-agostic conformations were smaller than those for the β-agostic conformation (back) by 3.2 kcal/mol on average. The energy difference of 3.2 kcal/mol roughly corresponds to the energetic difference between the α-agostic and β-agostic conformations of the resting state (Table 2). The contribution of the increased bulkiness was also observed in terms of the positional preference of the propylene methyl group. For example, when C_β was directed to the right side, the R_4 position became disadvantageous due to the steric repulsion with C_β, while the R_2 position was relatively free from the repulsion, and so on.

The coadsorption of EB further reduced the magnitudes of average ΔE_{ad} into –0.32 kcal/mol (Table 4). This destabilization partly originates from the prevention of the π electron donation from propylene due to the competitive electron donation from EB to $TiCl_2$*i*Bu. The steric repulsion between *i*Bu and EB also affected the ΔE_{ad} values greatly, since the growing chain tilts toward EB in the π complexation and sterically repulses with EB. The π complexation of propylene with the β-agostic conformations is sterically the most demanding to be least favored in the presence of EB. Among the α-agostic conformations, the right orientation of C_β (opposite to EB) combined with the placements of the propylene methyl group at R_1 or R_2 led to the least steric interference, thus giving the most stable species. On the contrary, the left orientation of C_β tended to be less favorable due to the steric repulsion between C_β and the carbonyl group of EB.

The ΔE_{ad} values calculated for the propylene π complexation with Ti-*i*Bu were always lower

than the entropic losses around 14 kcal/mol, estimated using a cluster model at 350 K. This fact assures that active sites are far from fully covered by propylene at typical polymerization temperatures, thus validating the usage of the apparent activation energies in subsequent insertion and chain transfer reactions [14,70]. Summing up the equilibrium populations calculated for different structures of the π complexes at 350 K (Tables 3 and 4), the equilibrium populations of the π complexes with specific enantiofaces of propylene or with specific conformations of the growing chain were given (Table 5). In the absence and even in the presence of EB, the adsorption of propylene was not enantioselective (similar populations for the *re* and *si* enantiofaces). This means that the stereoselectivity in propylene polymerization results solely from the stereoselectivity at the transition states of insertion. As for the conformations of the growing chain, the π complexes with the β-agostic conformation (back) were predominant in the absence of EB. However, the π complexes with the α-agostic conformation (right) became the main species in the presence of EB.

3.4. Influences of EB on the propylene insertion and chain transfer to propylene

As was mentioned in **3.1**, the Ti mononuclear species on the (110) surface and its coadsorption with donors are the most plausible scenarios, which can explain the experimentally observed electron donation picture and the amplification of C_2 symmetry around the Ti species by the addition of donors. Here, propylene polymerization performances of the Ti mononuclear species on the (110) surface were evaluated in the absence and in the presence of coadsorbed EB. For the validation of our scenarios, it is particularly important whether the Ti mononuclear species coadsorbed with EB on the (110) surface can reproduce experimentally observed effects

of donors such as improvements of iso- & regio-specificities and enlargement of polymer molecular weight [15,16,40-45,55,56].

Fig. 6 illustrates all the pathways examined for propylene insertion and chain transfer to propylene. The chain transfer to monomer is known as one of the major chain transfer pathways in the absence of hydrogen [78,79]. In order to fully consider stereo and regio aspects of these reactions, the position of the methyl group of propylene was varied at either of $R_{1\text{-}4}$. The placements of the methyl group at R_1 and R_2 correspond to the 1,2 orientation of propylene with the *re* and *si* prochiral planes, while those at R_3 and R_4 correspond to the 2,1 orientation with the the *re* and *si* prochiral planes, respectively. Propylene can react with Ti-*i*Bu in different ways according to the conformations of Ti-*i*Bu. When Ti-*i*Bu is situated in the α-agostic conformations, propylene can insert into the Ti-*i*Bu bond with the aid of the α-agostic interaction, as shown in Figs. 6a and 6b. In addition to the orientation of C_β either in the right or left side, the position of the methyl group at C_β was also varied either at R_A or R_B, where R_A and R_B are in the front and back sides against incoming propylene, respectively. In the case of the β-agostic conformation (back), propylene can insert with the aid of the β-agostic interaction (Fig. 6c). Differently from the other conformations, the β-agostic conformation (front) cannot be a precursor for the insertion. Instead, it can transfer β-hydrogen to incoming propylene, leading to the chain transfer to propylene (Fig. 6d). For the Ti-Me, only the α-agostic assisted insertion is feasible (Fig. 6e).

Table 6 corrects apparent activation energies (ΔE_{ap}) calculated for all the examined pathways in the absence of EB. The 1,2 insertion of propylene into Ti-Me required 2.1 kcal/mol of ΔE_{ap}, regardless of the prochiral faces. The ΔE_{ap} value for the ethylene insertion was –0.1 kcal/mol,

and that for the 1,2 insertion of fluoroethylene was 3.0 kcal/mol (on average). An inserting olefin molecule gets polarized as a result of the π-π* mixing at the transition state: the carbon atom of olefin that is bonding to C_α charges positively, while the carbon atom that is bonding to Ti charges negatively [3,76,80]. Substituents of olefin electrostatically affect the stability of the polarization at the transition state. An electron-withdrawing substituent at olefin further withdraws electron density from positively charged C_2 at the transition state of 1,2 insertion and thus destabilizes it, while an electron-donating substituent electrostatically stabilize the transition state of 1,2 insertion. Accordingly, the highest ΔE_{ap} value calculated for the 1,2 insertion of fluoroethylene is simply explained with the electrostatic reason. On the other hand, the higher ΔE_{ap} value for the 1,2 insertion of propylene than for the ethylene insertion must be attributed to steric congestion at the transition state, which exceeds the electrostatic contribution. The ΔE_{ap} values for the 2,1 insertion of propylene were 3.2-3.3 kcal/mol (again without prochiral preference), 1.1 kcal/mol higher than those for the 1,2 insertion. Thus the Ti mononuclear species is moderately regioselective even in the absence of donors. Though high propensity of $MgCl_2$-supported ZN catalysts for the 1,2 insertion is well known [15,44,45], its origin has not been fully understood yet. So far, two different explanations have been theoretically made for cationic Ti(VI) homogeneous systems [76,81]. One is a steric origin that the methyl group of propylene repulses with ligands located on both sides of the Ti center in the 2,1 insertion. The other is an electronic origin that the electron-donating methyl group destabilizes the transition state of the 2,1 insertion by further donating electron density into negatively-charged C_2. Judging from the fact that only quantum chemical calculations have succeeded to reproduce clear preference to the 1,2 insertion in heterogeneous systems

[44,49,70] (while molecular mechanics calculations failed [30]), the electronic origin must be very important. In our additional calculations using chloroethylene having electron-withdrawing Cl (whose size is similar to the methyl group for propylene), the 1,2 insertion was still advantageous but only by 0.6 kcal/mol over the 2,1 insertion. Thus, both the electrostatic and steric contributions are believed to be important for the regiospecificity of ZN catalysts.

In the previous section, the replacement of Ti-Me by Ti-*i*Bu largely reduced the magnitude of ΔE_{ad} for the π complexation of propylene, which was due to the stabilization of the resting state through the β-agostic interaction and due to the increase of the bulkiness around Ti. The latter factor also introduced energetic preferences toward specific conformations of π complexes in order to minimize steric congestion. Similar consequences were obtained for the propylene insertion. The replacement of Ti-Me by Ti-*i*Bu gave rise to the increase of ΔE_{ap} by 7.5 kcal/mol on average, while the degree of the increase was dependent on the mutual conformations of the growing chain and propylene. Among α-agostic assisted insertion pathways, the anti placement of the methyl group of propylene with respect to the C_α-C_β bond is favored for the 1,2 insertion, while the syn placement is favored for the 2,1 insertion [29,49,77]. It was also found that the methyl group at C_β of the growing chain was preferentially placed at R_B (*i.e.* in the back side of propylene) to reduce the steric congestion. As a consequence of these conformational restrictions, two 1,2 insertion pathways had the similarly lowest ΔE_{ap} values, *ca.* 7.4 kcal/mol, which is comparable with the experimentally determined activation enthalpies for the propylene insertion (9-12 kcal/mol) [14,82,83], assuring the validity of the employed model and method in this study. The two pathways are identical in terms of the anti placement of the propylene methyl group and the location of the C_β methyl group at R_B, while the orientation of the

growing chain is opposite. This fact indicates that the Ti mononuclear species on the (110) surface is aspecific (as has been conventionally believed) due to the inability to distinguish the orientation of the growing chain. As for the 2,1 insertion, the above-mentioned conformational restrictions were rather small since the propylene methyl group does not largely interfere with the growing chain. The energetically accessible pathways mostly had the C_β methyl group at R_B, whose average ΔE_{ap} value, 8.9 kcal/mol, was 1.5 kcal/mol greater than the lowest 1,2 insertion energies, *i.e.* moderately regioselective. A similar energetic difference (1.1-1.3 kcal/mol) between the 1,2 and 2,1 insertion was previously reported in non-local DFT calculations [44,49]. The β-agostic assisted 1,2 insertion exhibited similar ΔE_{ap} values to the most preferable α-agostic assisted pathways, indicating that the 1,2 insertion of propylene can occur via both types of the agostic assistances in the absence of EB. On the contrary, the β-agostic assisted 2,1 insertion was disadvantageous compared with the α-agostic assisted 2,1 insertion, plausibly because the strong β-agostic interaction increases the electron density of Ti and thus electrostatically destabilizes the 2,1 insertion.

The β-agostic conformation (front) leads to the chain transfer reaction to propylene. The activation energies calculated for the four chain transfer pathways having different propylene methyl placements are shown in Table 6. On the contrary to the insertion, the 1,2 placements of the propylene methyl group (at $R_{1,2}$) were disadvantageous for the chain transfer. The chain transfer energies with the 2,1 placement (at $R_{3,4}$) were as low as the lowest 1,2 insertion energies, indicative of a very low polymerization degree in the absence of EB.

Table 7 lists the ΔE_{ap} values in the presence of an EB molecule coadsorbed at the nearest Mg^{2+} site (S_A). The 1,2 insertion of propylene into Ti-Me required on average 3.3 kcal/mol of

ΔE_{ap}, being 1.1 kcal/mol higher than in the absence of EB. Though the *si* prochiral orientation of propylene (R_2) was preferred over the *re* prochiral orientation (R_1), the preference was as small as *ca.* 0.5 kcal/mol to regard the steric influence of EB as secondary. Therefore, the increase of the ΔE_{ap} values for Ti-Me was attributed mainly to the electrostatic destabilization of the transition states, where the enhanced electron density at Ti restricted the π donation and the resultant activation of the double bond. Sacchi et al. [41] showed that the stereoselectivity of the first propylene insertion into Ti-Et was much lower than the average stereoselectivity in the main chain, while that into Ti-*i*Bu was as high as the average stereoselectivity in the main chain. Thus, the calculated small energy difference between the two prochiral planes of the insertion into Ti-Me is consistent with their experimental observation that alkyl groups smaller than *i*Bu do not have sufficient repulsion with a bulky ligand, leading to lower stereoselectivity.

The average ΔE_{ap} value for the 2,1 insertion into Ti-Me was 5.3 kcal/mol to be 2.0 kcal/mol greater than that for the 1,2 insertion. Compared with the regiospecificity of 1.1 kcal/mol in the absence of EB, the coadsorption of EB obviously increased the regiospecificity of the Ti mononuclear species. Similar ΔE_{ap} values for the *re* and *si* prochiral orientations imply that the enhancement of the regiospecificity by EB is not caused by steric repulsion between the side Cl ion (forwarded to propylene by EB) and the methyl group of propylene. Most plausibly, the additional electron transfer from EB to Ti further enlarged electrostatic repulsion between the Ti center and C_2 carbon for the 2,1 insertion so as to destabilize it compared with the 1,2 insertion.

For Ti-*i*Bu, comparison of the corresponding ΔE_{ap} values in the absence and presence of EB (Tables 6 and 7) revealed that the coadsorption of EB basically increased the ΔE_{ap} values. The degree of the increase was dependent on the conformation of the growing chain as well as on

the positions of the methyl groups for Ti-*i*Bu. First, the β-agostic assisted insertion and the chain transfer to propylene, both having the β-agostic conformations as direct precursor, were significantly destabilized by the coadsorption of EB. The increases of the ΔE_{ap} values were, on average, 7.3 kcal/mol for the former and 4.8 kcal/mol for the latter. The destabilization of the α-agostic assisted insertion pathways, having the α-agostic conformations as direct precursor, was less, but the way of the destabilization was not uniform. The average ΔE_{ap} value became 1.57 kcal/mol higher for the pathways having the growing chain oriented toward the opposite (right) side of EB, and 2.12 kcal/mol for the growing chain oriented toward the EB (left) side, as compared with the corresponding pathways in the absence of EB. On the other hand, the average ΔE_{ap} value increased by 1.68 kcal/mol for the 1,2 insertion and 2.12 kcal/mol for the 2,1 insertion (among the α-agostic assisted insertion). Thus, EB not only sterically biases the orientation of the growing chain, but also electrostatistically prevents the 2,1 regio-misinsertion.

The pathway having the lowest ΔE_{ap} value possessed the positions of the methyl groups at R_2 (*si*) and at R_B, and the orientation of the growing chain to the right side. Its ΔE_{ap} value, 7.9 kcal/mol, was only *ca.* 0.5 kcal/mol higher than that of the corresponding pathway in the absence of EB, as a result of minimal steric interference. On the other hand, the pathway having the left-oriented growing chain as well as the placements of the methyl groups at R_1 (*re*) and R_B was destabilized by *ca.* 2.8 kcal/mol, due to stronger steric repulsion between the growing chain and EB. Consequently, the lowest ΔE_{ap} value for the 1,2-*re* insertion became 2.3 kcal/mol higher than that for the 1,2-*si* insertion, indicating that the nearest coadsorption of EB transforms the aspecific Ti mononuclear species into isospecific one. Our previous calculations using a small $MgCl_2$ cluster [77] revealed significant influences of the rigidity of the Mg-carbonyl bond on

the isospecificity, where fully relaxed EB never improved the isospecificity, while the fixation of the positions of the carbonyl group during propylene insertion resulted in high isospecificity. Meanwhile, the present calculations using thick $MgCl_2$ slab led to a different conclusion that a fully relaxed EB molecule can enhance the isospecificity. This deviation arises from the difference of the $MgCl_2$ models, where a small $MgCl_2$ cluster underestimated the rigidity of the Mg-carbonyl bond. Thus, a sufficiently large $MgCl_2$ model (such as the slab employed here) is critically important for accurate description of the steric influence of donors in propylene insertion.

The coadsorption of EB expanded the difference of the lowest ΔE_{ap} values for the 1,2 and 2,1 insertion to 2.1 kcal/mol, as compared to 1.3 kcal/mol in the absence of EB. As long as we know, this result corresponds to the first reproduction of the experimentally observed improvement of the regiospecificity by the addition of donors. Previous DFT calculations reached a different conclusion that the placement of succinate molecules at the nearest Mg^{2+} ions did not affect the regiospecificity [49]. This deviation is attributed to a rather small $MgCl_2$ cluster in the previous study [49], which cannot fully account for the electron re-distribution among $MgCl_2$, Ti species and donors. Meanwhile, the previous [49] and present DFT studies coincided in the fact that the 2,1 insertion prefers the prochiral plane (*re*) opposite to the plane (*si*) preferred by the 1,2 insertion.

As a summary, EB coadsorbed at the nearest Mg^{2+} ion improved the isospecificity of the originally aspecific Ti mononuclear species through the steric repulsion with the growing chain, and the regiospecificity through the electron enrichment of the Ti species. Based on these mechanisms, it is naturally expected that the degrees of the improvements of the specificities are

dependent on methods and models employed. At least, a small $MgCl_2$ model could reach conclusions which were inconsistent with the experimentally observed effects of donors.

Table 8 shows equilibrium probabilities of different reactions at 350 K, and those of the conformations of the growing chain involved in the reactions at the same temperature, which were calculated based on the data in Tables 6 and 7. As was already described, the entropic contributions were assumed to be similar among the different reactions, and neglected in the calculations. In the absence of EB, both the 1,2 and 2,1 insertion is not stereoselective without capability to control the orientation of the growing chain. This is consistent with the conventional idea that the Ti mononuclear species on the $MgCl_2$ (110) surface is aspecific, lacking stereo-regulating ligands [25,47,49]. Though the 1,2 insertion is basically favored, the probability of the regio-misinsertion among the insertion is estimated to be *ca.* 15% in the absence of donors, which is much greater than the experimentally reported lowest regiospecificity, 1.5% for the hexane-soluble fraction of polypropylene in the absence of donors [44]. This might be explained by two factors: first, completely atactic polypropylene is never formed in actual heterogeneous ZN propylene polymerization, whose reason will be described later. Second, the regiospecificity is rather sensitive to the kind of DFT functionals [44]. The probability of the chain transfer to monomer as high as 26% suggests inability of the chain growth at the Ti mononuclear species on the (110) surface. This plausibly explains the reason why completely atactic polypropylene is never obtained in heterogeneous ZN propylene polymerization, and consistent with a known fact that less tactic polymer tends to be shorter and contain a larger content of end unsaturation [78]. The four kinds of the growing chain conformations are almost equally involved in the catalysis, although the resting state dominantly

exists as the β agostic conformations (Table 2).

The coadsorption of EB largely restricts the conformations of the growing chain which can be involved in the catalysis with propylene. Most prominently, the coadsorption prevents the β-agostic assisted pathways, which are sterically demanding. As a result, the probability of the chain transfer to monomer, the main cause to prevent the growth of completely atactic chain, drops to 0.5%. This result is consistent with the fact that more isotactic polymer tends to be longer and contain a smaller end unsaturation fraction [78]. The second consequence brought about by the coadsorption of EB is the restriction of the α-agostic insertion into the left-oriented growing chain, leading to a dramatic reduction of the probability for the 1,2-*re* insertion. The stereoregularity estimated from the calculated probabilities corresponds to 82 mol% of *mmmm*, rather lower than a typical experimental value (~95 mol%) [15]. However, considering the exponential sensitivity of *mmmm*, the estimation is regarded as quite reasonable. The probability of the 2,1 insertion moderately decreases from 15% to 6% by the coadsorption of EB. Though the probability of 6% is still much higher than experimentally estimated regioselectivity [44,45], it is more important that we could firstly reproduce the improvement of the regiospecificity in the presence of donors. As was mentioned, one of the purposes of the present study is to qualitatively depict the steric and electronic influences of donors on propylene polymerization by means of comprehensive DFT calculations. In this sense, the model based on the nearest coadsorption of donors (as well as the employed methods) totally succeeded to reproduce experimentally known improvements of stereo- and regio-specificities, and increase of molecular weight by the addition of donors [15,16,40-45,55,56], allowing us to propose a working active site model, so called “coadsorption model.”

4. Conclusions

A series of periodic DFT calculations have been conducted to conclude on the mechanism for donors to influence polymerization performances of $MgCl_2$-supported ZN catalysts. Systematic and exclusive calculations based on appropriate levels of methods and $MgCl_2$ models have been performed not only on the states and interactions of the catalytic components but also on their influences on the polymerization performances, and the obtained results were validated in terms of various experimental aspects. Major findings are described as follows.

- Considering that donors stabilize active $MgCl_2$ surfaces to increase their fractions during preparation [23,24], diether-type donors are expected to form (110)-rich $MgCl_2$, while mono- and di-ester-type donors can form $MgCl_2$ exposing both the (110) and (100) surfaces. In both of the cases, $TiCl_4$ tends to adsorb on the (110) surface.
- The mutual location of $TiCl_4$ and donors on the (110) surface is energetically randomly decided, and they tend to coadsorb close to each other at a high surface coverage, which is the case for real catalysts.
- The coadsorption of $TiCl_4$ and donors on the (110) surface not only reproduces experimentally observed enrichments of the Ti electron density in the presence of $MgCl_2$ and donors [53,54], but also explains the amplification of C_2 symmetry around the Ti species as a result of random placements of donors.
- In the absence of donors, the Ti mononuclear species on the (110) surface is totally aspecific without capability to distinguish the orientation of the growing chain at the transition state, while it is moderately regiospecific favoring the 1,2 insertion. The chain

transfer to propylene is as facile as the insertion, indicating no chain growth at the completely aspecific Ti mononuclear species.

- The nearest coadsorption of EB i) converts the aspecific Ti mononuclear species into isospecific one by sterically controlling the orientation of the growing chain at the transition state, ii) improves the regiospecificity as a result of increased electrostatic repulsion for the 2,1 insertion, iii) and dramatically prevents chain transfer to propylene, thus enabling the chain growth at the Ti mononuclear species.

In this way, it was successfully proven that the coadsorption of donors with the Ti mononuclear species on the $MgCl_2$ (110) surface is not only energetically plausible but also can reproduce a number of experimental facts such as the enhancements of iso- and regio-specificities and molecular weight by the addition of donors. The proposed "coadsorption model" gives a comprehensive molecular-level description for the roles of donors as well as a scientific basis for the first-principle prediction of new donor structures.

Acknowledgement

This work was financially supported by Grants-in-Aid for Scientific Research from Japan Society for the Promotion of Science, Japan Polypropylene Corporation, Samsung Total Petrochemicals Co., Ltd., Sumitomo Chemical Co., Ltd., and Toho Titanium Co., Ltd.

References

[1] H. Sinn, W. Kaminsky, Adv. Organomet. Chem. 18 (1980) 99.

[2] D.J. Arriola, E.M. Carnahan, P.D. Hustad, R.L. Kuhlman, T.T. Wenzel, Science 312 (2006)

714.

[3] L. Resconi, L. Cavallo, A. Fait, F. Piemontesi, Chem. Rev. 100 (2000) 1253.

[4] L.S. Boffa, B.M. Novak, Chem. Rev. 100 (2000) 1479.

[5] V.C. Gibson, S.K. Spitzmesser, Chem. Rev. 103 (2003) 283.

[6] G.W. Coates, Chem. Rev. 100 (2000) 1223.

[7] M.B. Harney, Y. Zhang, L.R. Sita, Angew. Chem. Int. Ed. 45 (2006) 6140.

[8] M. Delferro, T.J. Marks, Chem. Rev. 111 (2011) 2450.

[9] T.R. Younkin, E.F. Conner, J.I. Henderson, S.K. Friedrich, R.H. Grubbs, D.A. Bansleben, Science 287 (2000) 460.

[10] H. Makio, N. Kashiwa, T. Fujita, Adv. Synth. Catal. 344 (2002) 477.

[11] T.C. Chung, Prog. Polym. Sci. 27 (2002) 39.

[12] L. Luciani, N. Kashiwa, P.C. Barbe, A. Toyota, Ger. Patent 2 643 143 (1977), to Montedison and Mitsui Petrochemical.

[13] K. Czaja, B. Król, Polimery 43 (1998) 287.

[14] T. Keii, Heterogeneous Kinetics: Theory of Ziegler-Natta-Kaminsky Polymerization, Kodansha, Tokyo, 2004, p. 113.

[15] E. Albizzati, U. Giannini, G. Collina, L. Noristi, L. Resconi, in: E.P. Moore, Jr. (Ed.), Polypropylene Handbook, Hanser-Gardner Publications: Cincinnati, OH, 1996, p. 11.

[16] G. Cecchin, G. Morini, A. Pelliconi, Macromol. Symp. 173 (2001) 195.

[17] U. Giannini, Makromol. Chem. Suppl. 5 (1981) 216.

[18] R. Zannetti, C. Marega, A. Marigo, A. Martorana, J. Polym. Sci. Part B: Polym. Phys. 26 (1988) 2399.

[19] V. Busico, M. Causà, R. Cipullo, R. Credendino, F. Cutillo, N. Friederichs, R. Lamanna, A. Segre, V. Van Axel Castelli, J. Phys. Chem. C 112 (2008) 1081.

[20] E. Magni, G.A. Somorjai, Appl. Surf. Sci. 89 (1995) 187.

[21] E. Magni, G.A. Somorjai, Surf. Sci. 341 (1995) L1078.

[22] H. Mori, M. Sawada, T. Higuchi, K. Hasebe, N. Otsuka, M. Terano, Macromol. Rapid Commun. 20 (1999) 245.

[23] A. Andoni, J.C. Chadwick, J.W. Niemantsverdriet, P.C. Thüne, J. Catal. 257 (2008) 81.

[24] R. Credendino, J.T.M. Pater, A. Correa, G. Morini, L. Cavallo, J. Phys. Chem. C 115 (2011) 13322.

[25] V. Busico, P. Corradini, L. De Martino, A. Proto, V. Savino. E. Albizzati, Makromol. Chem. 186 (1985) 1279.

[26] Y.I. Yermakov, V.A. Zakharov, Adv. Catal. 24 (1976)173.

[27] K. Soga, T. Sano, R. Ohnishi, Polym. Bull. 4 (1981) 157.

[28] K. Soga, S.I. Chen, R. Ohnishi, Polym. Bull. 8 (1982) 473.

[29] P. Corradini, G. Guerra, R. Fusco, V. Barone, Eur. Polym. J. 16 (1980) 835.

[30] P. Corradini, V. Barone, R. Fusco, G. Guerra, J. Catal. 77 (1982) 32.

[31] A.A.S. Filho, M.C.M. Alves, J.H.Z. Santos, J. Appl. Polym. Sci. 109 (2008) 1675.

[32] L. Brambilla, G. Zerbi, F. Piemontesi, S. Nascetti, G. Morini, J. Mol. Catal. A: Chem. 263 (2007) 103.

[33] A.G. Potapov, V.V. Kriventsov, D.I. Kochubey, G.D. Bukatov, V.A. Zakharov, Macromol. Chem. Phys. 198 (1997) 3477.

[34] T. Taniike, M. Terano, Macromol. Rapid. Commun. 29 (2008) 1472.

[35] G. Monaco, M. Toto, G. Guerra, P. Corradini, L. Cavallo, Macromolecules 33 (2000) 8953.

[36] C. Martinsky, C. Minot, J.M. Ricart, Surf. Sci. 490 (2001) 237.

[37] D.V. Stukalov, I.L. Zilberberg, V.A. Zakharov, Macromolecules 42 (2009) 8165.

[38] M. Boero, M. Parrinello, H. Weiss, S. Hüffer, J. Phys. Chem. A 105 (2001) 5096.

[39] M. D'Amore, R. Credendino, P.H.M. Budzelaar, M. Causà, V. Busico, J. Catal. 286 (2012) 103.

[40] A. Zambelli, P. Ammendola, Prog. Polym. Sci. 16 (1991) 203.

[40] M.C. Sacchi, I. Tritto, P. Locatelli, Prog. Polym. Sci. 16 (1991) 331.

[42] J.C. Chadwick, G. Morini, G. Balbontin, I. Camurati, J.J.R. Heere, I. Mingozzi, F. Testoni, Macromol. Chem. Phys. 202 (2001) 1995.

[43] T. Wada, T. Taniike, I. Kouzai, S. Takahashi, M. Terano, Macromol. Rapid Commun. 30 (2009) 887.

[44] V. Busico, R. Cipullo, C. Polzone, G. Talarico, J.C. Chadwick, Macromolecules 36 (2003) 2616.

[45] V. Busico, J.C. Chadwick, R. Cipullo, S. Ronca, G. Talarico, Macromolecules 37 (2004) 7437.

[46] M. Terano, T. Kataoka, T. Keii, Macromol. Chem. 188 (1987) 1477.

[47] V. Busico, R. Cipullo, G. Monaco, G. Talarico, M. Vacatello, J.C. Chadwick, A.L. Segre, O. Sudmeijer, Macromolecules 32 (1999) 4173.

[48] B. Liu, T. Nitta, H. Nakatani, M. Terano, Macromol. Chem. Phys. 204 (2003) 395.

[49] A. Correa, F. Piemontesi, G. Morini, L. Cavallo, Macromolecules 40 (2007) 9181.

[50] L. Brambilla, G. Zerbi, F. Piemontesi, S. Nascetti, G. Morini, J. Phys. Chem. C 114 (2010)

11475.

[51] T. Taniike, M. Terano, Macromol. Rapid. Commun. 28 (2007) 1918.

[52] T. Taniike, M. Terano, Macromol. Symp. 260 (2008) 98.

[53] K. Soga, T. Shiono, Prog. Polym. Sci. 22 (1997) 1503.

[54] X. Zhao, Y. Zhang, Y. Song, G. Wei, Surf. Rev. Lett. 14 (2007) 951.

[55] C.B. Yang, C.C. Hsu, J. Appl. Polym. Sci. 58 (1995) 1245.

[56] M.C. Sacchi, F. Forlini, I. Tritto, R. Mendichi, G. Zannoni, L. Noristi, Macromolecules 25 (1992) 5914.

[57] B. Delley, J. Chem. Phys. 92 (1990) 508.

[58] J.P. Perdew, K. Burke, M. Ernzerhof, Phys. Rev. Lett. 77 (1996) 3865.

[59] J.P. Perdew, Y. Wang, Phys. Rev. B 45 (1992) 13244.

[60] A.D. Becke, J. Chem. Phys. 88 (1988) 2547.

[61] C. Lee, W. Yang, R.G. Parr, Phys. Rev. B 37 (1988) 785.

[62] M. Dolg, U. Wedig, H. Stoll, H. Preuss, J. Chem. Phys. 86 (1987) 866.

[63] A. Bergner, M. Dolg, W. Kuechle, H. Stoll, H. Preuss, Mol. Phys. 80 (1993) 1431.

[64] L. Brambilla, G. Zerbi, S. Nascetti, F. Piemontesi, G. Morini, Macromol. Symp. 213 (2004) 287.

[65] E.J. Arlman, P. Cossee, J. Catal. 3 (1964) 99.

[66] M. Brookhart, M.L.H. Green, J. Organomet. Chem. 250 (1983) 395.

[67] M. Boero, M. Parrinello, K. Terakura, J. Am. Chem. Soc. 120 (1998) 2746.

[68] L. Cavallo, G. Guerra, P. Corradini, J. Am. Chem. Soc. 120 (1998) 2428.

[69] M. Seth, T. Ziegler, Macromolecules 37 (2004) 9191.

[70] Z. Flisak, T. Ziegler, Macromolecules 38 (2005) 9865.

[71] M. Seth, T. Ziegler, Macromolecules 36 (2003) 6613.

[72] M. Toto, G. Morini, G. Guerra, P. Corradini, L. Cavallo, Macromolecules 33 (2000) 1134.

[73] S.A. Sergeev, V.A. Poluboyarov, V.A. Zakharov, V.F. Anufrienko, G.D. Bukatov, Makromol. Chem. 186 (1985) 243.

[74] P. Corradini, V. Busico, L. Cavallo, G. Guerra, M. Vacatello, V. Venditto, J. Mol. Catal. 74 (1992) 433.

[75] H. Kawamura-Kuribayashi, N. Koga, K. Morokuma, J. Am. Chem. Soc. 114 (1992) 8687.

[76] H. Kawamura-Kuribayashi, N. Koga, K. Morokuma, J. Am. Chem. Soc. 114 (1992) 2359.

[77] T. Taniike, M. Terano, Macromol. Chem. Phys. 210 (2009) 2188.

[78] T. Shiono, K.K. Kang, H. Hagihara, T. Ikeda, Macromolecules 30 (1997) 5997.

[79] J.C. Chadwick, J.J.R. Heere, O. Sudmeijer, Macromol. Chem. Phys. 201 (2000) 1846.

[80] P. Margl, L. Deng, T. Ziegler, J. Am. Chem. Soc. 120 (1998) 5517.

[81] G. Talarico, V. Busico, L. Cavallo, J. Am. Chem. Soc. 125 (2003) 7172.

[82] T. Keii, E. Suzuki, M. Tamura, M. Murata, Y. Doi, Makromol. Chem. 183 (1982) 2285.

[83] T. Keii, M. Terano, K. Kimura, K. Ishii, in: W. Kaminsky, H. Sinn (Eds.), Transition Metals and Organometallics as Catalysts for Olefin Polymerization, Springer-Verlag, Berlin, 1988, p. 3.

Figure captions

Fig. 1. Adsorption structures of $TiCl_4$ on $MgCl_2$ surfaces: a) mononuclear species on the (110) surface, and b) mononuclear and c) dinuclear species on the (100) surface. Black: Mg, white: Cl, purple: Ti.

Fig. 2. Adsorption structures of donors on $MgCl_2$ surfaces (only relevant atoms are shown). a,b) Benzoate adsorbed on the (110) and (100) surfaces in a monodentate fashion, c-e) phthalate adsorbed on the (110) surface in bidentate, intra-bridging, and inter-bridging fashions, f) phthalate adsorbed on the (100) surface in an intra-bridging mode. Black: Mg, white: Cl (balls) & H (sticks), gray: C, red: O. The color schemes in Figs. 1 and 2 are used in subsequent Figs.

Fig. 3. Origins of a C_2 symmetry and isospecificity of the Ti mononuclear species on the $MgCl_2$ (110) surface. a) Top view of Ti mononuclear active species on the (110) surface, where $S_{A\text{-}E'}$ describe Mg^{2+} sites available for the coadsorption of donors. The projection of the reaction space around the Ti species is schematically illustrated in the right side. Note that the two white and gray quadrants defined across the O_h axes of the Ti species are not equivalent in terms of the underlying $MgCl_2$ layers. b) Coadsorption of benzoate molecules at the sterically most important $S_{A,A'}$ sites to occupy the gray quadrants, and c) coadsorption of diester molecules at the sterically most important $S_{C,E,C'E'}$ sites to occupy the white quadrants.

Fig. 4. Conformations of the resting state at the Ti mononuclear species on the $MgCl_2$ (110) surface. a,b) α-agostic conformations with right and left orientations of the growing chain (*i*Bu),

and c,d) β-agostic conformations with back and front orientations of the growing chain. Hydrogen atoms relevant to the agostic interactions are yellow-colored. These conformations were examined both in the absence and presence of EB.

Fig. 5. Structures of π complexes between propylene and the Ti mononuclear active species on the $MgCl_2$ (110) surface. a,b) π complexes for the α-agostic conformations of the *i*Bu growing chain (right- and left-oriented), c,d) π complexes for the β-agostic conformations of the *i*Bu growing chain (back- and front-oriented), and e) π complexes for the Me growing chain. f) The position of the methyl group of propylene (yellow-colored) was varied at either of $R_{1\text{-}4}$, and the position of the methyl group at C_β of *i*Bu (blue-colored) was varied at either R_A or R_B. These structures were examined both in the absence and presence of EB.

Fig. 6. Pathways examined for propylene insertion and for chain transfer to propylene at the Ti mononuclear active species on the $MgCl_2$ (110) surface. a,b) Insertion into Ti-*i*Bu with the α-agostic conformations (right- and left-oriented), c) insertion into Ti-*i*Bu with the β-agostic conformation (back-oriented), d) chain transfer to propylene, and e) insertion into Ti-Me. f) The positions of the methyl groups of propylene and at C_β of *i*Bu were similarly varied. These pathways were examined both in the absence and presence of EB.

Table 1

Adsorption energies of $TiCl_4$ and internal donors on $MgCl_2$ surfaces.

$MgCl_2$ surface	Adsorbate	Structure	ΔE_{ad} [kcal/mol]
(110)	$TiCl_4$	Mononuclear	–19.8
	Benzoate[a]	Monodentate	–29.8
	Phthalate[a]	Bidentate[b]	–38.8
		Intra-layer bridge[b]	–32.5
		Inter-layer bridge[b]	–33.7
	Succinate[a]	Bidentate[b]	–38.6
		Intra-layer bridge[b]	–36.9
		Inter-layer bridge[b]	–43.3
	1,3-diether[a]	Bidentate[b]	–31.1
(100)	$TiCl_4$	Mononuclear	–13.0
		Dinuclear	–11.1
	Benzoate[a]	Monodentate	–30.5
	Phthalate[a]	Intra-layer bridge[b]	–42.4
	Succinate[a]	Intra-layer bridge[b]	–45.0
	1,3-diether[a]	Intra-layer bridge[b]	–7.5

[a] Benzoate: ethylbenzoate (EB); phthalate: diethylphthalate; succinate: (2R,3R)-2,3-diisopropyldiethylsuccinate; 1,3-diether: 2,2-diisopropyl-1,3-dimethoxypropane.

[b] "Bidentate" is sometimes called as "chelate". "Intra-layer bridge" and "inter-layer bridge" correspond to bridging adsorption of donors within one $MgCl_2$ layer and between two neighboring $MgCl_2$ layers, respectively. The latter is also called as "zip" [49].

Table 2

Stability of different conformations of the resting state in the absence and presence of EB.

Conformation[a]	Relative stability [kcal/mol][b]	
	Without EB	With EB
α-agostic (right)	3.95 (0.19%)	7.58 (1.30%)
α-agostic (left)	3.90 (0.20%)	7.17 (2.33%)
β-agostic (back)	0.00 (55.6%)	5.62 (22.0%)
β-agostic (front)	0.16 (44.0%)	4.77 (74.4%)
Me[c]	0.00	3.12

[a] The corresponding structures are shown in Fig. 4.

[b] The relative stability of each conformation was calculated by setting the energy of the most stable β-agostic conformation (back) in the absence of EB as the zero-point energy. The stability of each conformation in the presence of EB was derived by $\{E(TiCl_2iBu/EB/MgCl_2) - E(TiCl_2iBu/MgCl_2)\} - \{E(TiCl_3/EB/MgCl_2) - E(TiCl_3/MgCl_2)\}$. The values in the parenthesis are the equilibrium populations of the corresponding conformations at 350 K.

[c] Me was used instead of *i*Bu.

Table 3

π complexation energies of propylene in the absence of EB[a].

Growing chain	ΔE_{ad} [kcal/mol][b]			
	R_1 (*re*)	R_2 (*si*)	R_3 (*re*)	R_4 (*si*)
α-agostic (right, R_A)	–2.24 (0.22%)	–3.52 (1.43%)	–1.01 (0.04%)	–1.86 (0.13%)
α-agostic (right, R_B)	–1.62 (0.09%)	–3.04 (0.71%)	–3.27 (0.99%)	–1.72 (0.11%)
α-agostic (left, R_A)	–0.73 (0.03%)	–3.40 (1.21%)	–3.63 (1.67%)	–2.76 (0.48%)
α-agostic (left, R_B)	–0.26 (0.01%)	–2.40 (0.28%)	–2.17 (0.20%)	–1.55 (0.08%)
β-agostic (back)	**–5.77** (**36.4%**)	**–5.33** (**19.2%**)	**–5.27** (**17.7%**)	**–5.23** (**16.8%**)
β-agostic (front)	–2.66 (0.41%)	–2.36 (0.27%)	–2.73 (0.45%)	–3.36 (1.13%)
Me[c]	–8.14 (11.5%)	–8.89 (33.6%)	–8.87 (32.9%)	–8.59 (21.9%)

[a] The corresponding structures are shown in Fig. 5.

[b] The adsorption energy (ΔE_{ad}) of propylene was calculated based on E(π complex) – {E(the most stable resting state) + E(gaseous propylene)}. The values in the parenthesis are the equilibrium populations of the corresponding adsorption states at 350 K.

[c] Me was used instead of *i*Bu. ΔE_{ad} of ethylene was –9.45 kcal/mol and ΔE_{ad} of fluoroethylene (on average) was –6.37 kcal/mol for Ti-Me.

Table 4

π complexation energies of propylene in the presence of EB.

Growing chain	ΔE_{ad} [kcal/mol]			
	R_1 (*re*)	R_2 (*si*)	R_3 (*re*)	R_4 (*si*)
α-agostic (right, R_A)	**–2.39** (**25.4%**)	–1.38 (5.96%)	0.29 (0.54%)	0.67 (0.31%)
α-agostic (right, R_B)	–1.15 (4.26%)	**–2.23** (**20.4%**)	–0.88 (2.92%)	–0.12 (0.97%)
α-agostic (left, R_A)	0.02 (0.79%)	–0.62 (2.00%)	–0.11 (0.95%)	**–1.81** (**11.0%**)
α-agostic (left, R_B)	–0.31 (1.27%)	–1.48 (6.91%)	–0.56 (1.83%)	–0.77 (2.46%)
β-agostic (back)	–1.65 (8.83%)	1.53 (0.09%)	2.13 (0.04%)	–0.62 (2.00%)
β-agostic (front)	0.55 (0.37%)	1.71 (0.07%)	0.76 (0.27%)	0.64 (0.33%)
Me[a]	–6.67 (33.8%)	–5.93 (11.6%)	–5.25 (4.35%)	–6.95 (50.3%)

[a] ΔE_{ad} of ethylene was –7.98 kcal/mol and ΔE_{ad} of fluoroethylene (on average) was –5.41 for Ti-Me.

Table 5

Equilibrium populations of the π complexes with specific enantiofaces of propylene or with specific conformations of the growing chain[a].

Conformation	Without EB	With EB
$R_{1,3}$ (*re*)[b]	58.2%	47.5%
$R_{2,4}$ (*si*)[b]	41.8%	52.5%
α-agostic (right)[c]	3.72%	60.8%
α-agostic (left)[c]	3.97%	27.2%
β-agostic (back)[c]	90.1%	11.0%
β-agostic (front)[c]	2.26%	1.03%

[a] Calculated based on the equilibrium populations of the π complexes at 350 K in Tables 3 and 4.

[b] Summation over all the π complexes with specific enantiofaces of propylene (irrespectively of the conformations of the growing chain).

[c] Summation over all the π complexes with specific conformations of the growing chain (irrespectively of the propylene enantiofaces).

Table 6

Apparent activation energies of propylene insertion and chain transfer to propylene in the absence of EB[a].

Growing chain	ΔE_{ap} [kcal/mol][b]			
	R_1 (*re*)	R_2 (*si*)	R_3 (*re*)	R_4 (*si*)
α-agostic (right, R_A)	15.4 (0.00%)	9.20 (1.34%)	10.8 (0.13%)	9.45 (0.93%)
α-agostic (right, R_B)	14.2 (0.00%)	**7.36** (**18.9%**)	8.82 (2.31%)	9.39 (1.02%)
α-agostic (left, R_A)	9.71 (0.64%)	11.3 (0.06%)	10.8 (0.13%)	14.5 (0.00%)
α-agostic (left, R_B)	**7.52** (**15.0%**)	12.8 (0.01%)	8.66 (2.91%)	8.90 (2.06%)
β-agostic (back)	**7.91** (**8.57%**)	**7.37** (**18.7%**)	9.21 (1.32%)	11.0 (0.10%)
β-agostic (front)[c]	8.42 (4.11%)	8.49 (3.72%)	**7.63** (**12.8%**)	8.26 (5.18%)
Me[d]	2.15 (39.4%)	2.07 (44.2%)	3.18 (8.94%)	3.31 (7.41%)

[a] The corresponding pathways are shown in Fig. 6.

[b] The zero-point energy to calculate the apparent activation energies was set to the total energy of the most stable resting state and gaseous propylene [14,70]. The values in the parenthesis are the probabilities of the corresponding pathways at 350 K.

[c] Chain transfer to propylene.

[d] Me was used instead of *i*Bu. ΔE_{ap} for ethylene insertion was calculated to be –0.07 kcal/mol, and ΔE_{ap} for the 1,2 insertion of fluoroethylene was on average 2.95 kcal/mol.

Table 7

Apparent activation energies of the propylene insertion and chain transfer to propylene in the presence of EB.

Growing chain	ΔE_{ap} [kcal/mol]			
	R_1 (*re*)	R_2 (*si*)	R_3 (*re*)	R_4 (*si*)
α-agostic (right, R_A)	16.8 (0.00%)	9.90 (4.26%)	12.6 (0.09%)	11.5 (0.41%)
α-agostic (right, R_B)	16.5 (0.00%)	**7.90** (**76.0%**)	**9.07** (**14.1%**)	11.9 (0.24%)
α-agostic (left, R_A)	11.7 (0.31%)	13.9 (0.01%)	13.5 (0.02%)	15.3 (0.00%)
α-agostic (left, R_B)	10.2 (2.89%)	14.0 (0.01%)	11.6 (0.37%)	11.0 (0.86%)
β-agostic (back)	13.8 (0.02%)	14.4 (0.01%)	17.6 (0.00%)	18.7 (0.00%)
β-agostic (front)	12.6 (0.09%)	12.8 (0.07%)	11.9 (0.25%)	14.7 (0.00%)
Me[a]	3.51 (31.7%)	3.03 (63.4%)	5.31 (2.37%)	5.26 (2.55%)

[a] Me was used instead of *i*Bu. ΔE_{ap} for the ethylene insertion was 1.50 kcal/mol, and ΔE_{ap} for the 1,2 insertion of fluoroethylene was on average 4.29 kcal/mol.

Table 8

Equilibrium probabilities for the reactions and for the conformations of the growing chain involved in the reactions[a].

Conformation	Without EB	With EB
1,2-*re* insertion[b]	24.3%	3.59%
1,2-*si* insertion[b]	39.0%	89.6%
2,1-*re* insertion[b]	6.79%	4.71%
2,1-*si* insertion[b]	4.11%	1.69%
chain transfer to propylene[c]	25.8%	0.46%
α-agostic (right)[d]	24.7%	94.5%
α-agostic (left)[d]	20.8%	4.99%
β-agostic (back)[d]	28.7%	0.03%
β-agostic (front)[d]	25.8%	0.46%

[a] Calculated based on the equilibrium probabilities of different pathways at 350 K in Tables 6 and 7.

[b] Summation over all the 1,2 or 2,1 insertion pathways with the *re* or *si* prochiral plane.

[c] Summation over all the chain transfer pathways to propylene.

[d] Summation over the pathways with specific conformations of the growing chain.

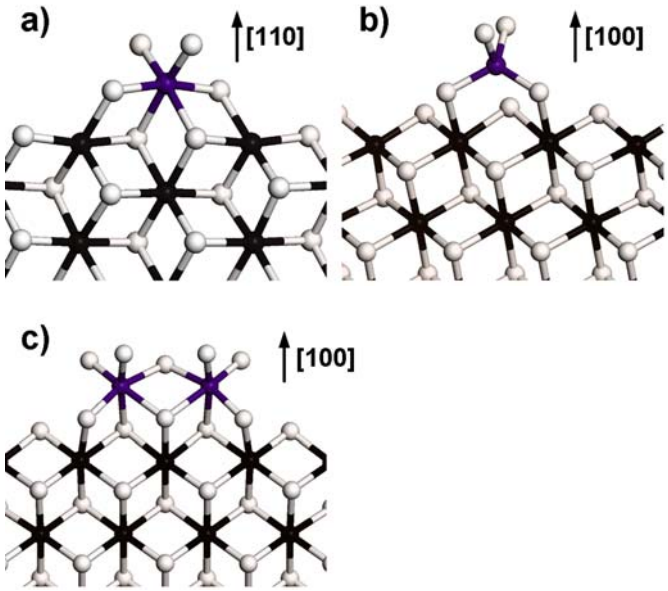

Fig. 1.

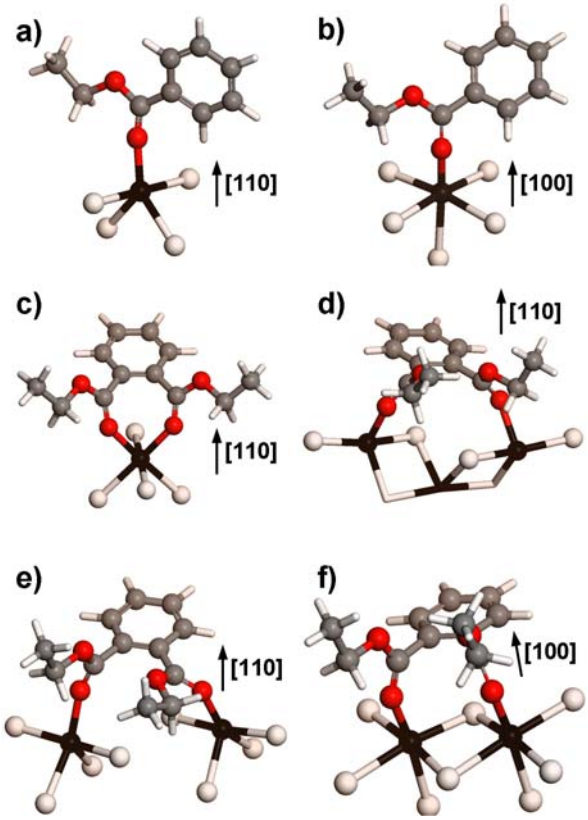

Fig. 2.

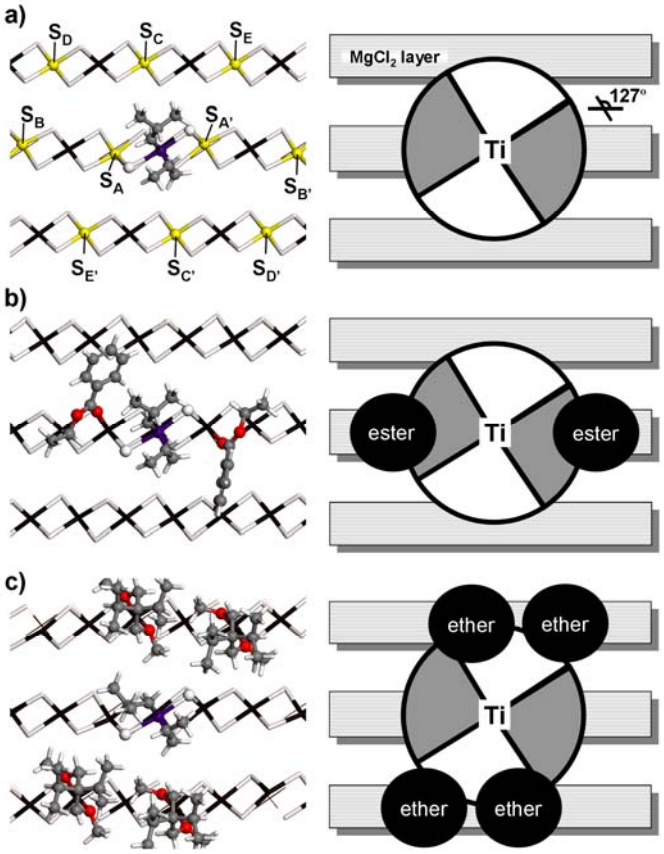
a)
S_D
S_C
S_E
S_B
$S_{A'}$
S_A
$S_{B'}$
$S_{E'}$
$S_{C'}$
$S_{D'}$
$MgCl_2$ layer
127°
Ti
b)
ester
Ti
ester
c)
ether
ether
Ti
ether
ether

Fig. 3.

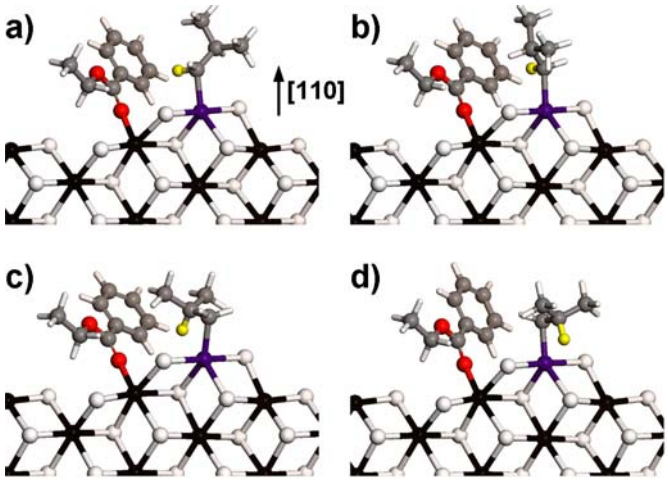
a)
[110]
b)
c)
d)

Fig. 4.

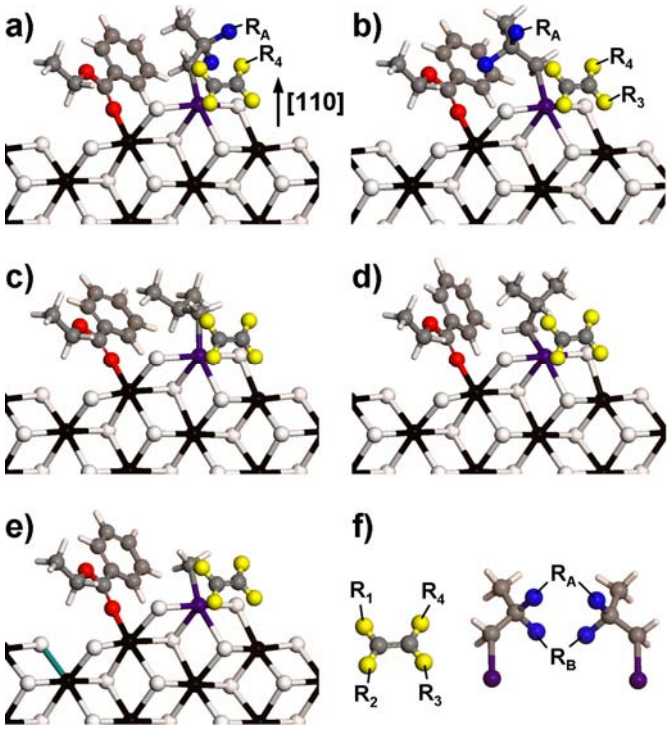
a)
R_A
R_4
[110]
b)
R_A
R_4
R_3
c)
d)
e)
f)
R_1
R_4
R_2
R_3
R_A
R_B

Fig. 5.

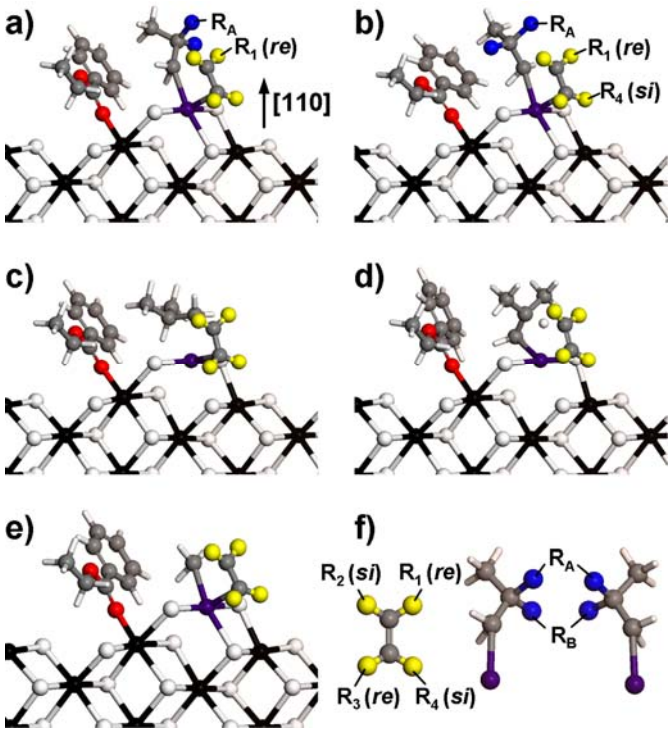
a)
R_A
R_1 (*re*)
[110]
b)
R_A
R_1 (*re*)
R_4 (*si*)
c)
d)
e)
f)
R_2 (*si*)
R_1 (*re*)
R_3 (*re*)
R_4 (*si*)
R_A
R_B

Fig. 6.